GUST FRONT DETECTION USING NEURO-FUZZY ALGORITHM WITH POLARIMETRIC WSR-88D

Amber J. Liggett[1,2] and Tian-You Yu[3]

[1]National Weather Center Research Experiences for Undergraduates Program
Norman, Oklahoma

[2] Department of Earth Sciences, Millersville University
Millersville, Pennsylvania

[3]Advanced Radar Research Center and School of Electrical and Computer Engineering,
University of Oklahoma, Norman, Oklahoma

ABSTRACT

The strong wind, shear, and turbulence associated with gust fronts can negatively impact aircraft operations at terminals, vegetation and other structures. Currently, the Machine Intelligence Gust-Front detection Algorithm (MIGFA) identifies gust front based on signatures from Doppler radar measurements. The upgrade of the Weather Surveillance Radar-1988 Doppler (WSR-88D) network to polarimetric capabilities was recently completed in 2013. Therefore it is timely to exploit the additional polarimetric measurements to improve gust front detection. The Neuro-Fuzzy Gust-front Detection Algorithm (NFGDA) was developed for this task. NFGDA preliminary results yielded a higher performance than MIGFA, motivating this study to investigate more gust front cases to confirm polarimetric signatures of gust fronts and verify the performance of NFGDA. In this study, eight gust front cases are identified and analyzed using the NFGDA. Findings included similarities between these and preliminary polarimetric gust front signatures. Additionally, the performance results yielded suggested refinements based on the statistical analysis of the algorithm. More specific guidelines can be placed in defining a gust front, as it is not a well-defined storm feature. Overall, there is room for improvement in order to alleviate this defect of the promising algorithm.

1. INTRODUCTION

A gust front (GF) is a propagating boundary of a parent storm caused by the descending, cold, and dense air from a storm that is pushing surrounding air at the surface. In other words, it is produced as the storm downdraft reaches the ground and spreads horizontally (Klingle et al. 1987). GFs can be observed by radar because of intensified reflectivity (compared to clear-air echoes) and velocity characteristics (Rinehart 2004).

The typical wind gusts associated gust front are 20 ms^{-1} (up to 40 ms^{-1}) and the propagation speed of GFs ranges between 5-20 ms^{-1}. A GF can exceed 12 km in length and 1 km in width. Its traveling distance extends to tens of kilometers over a duration of several hours. The fronts produce low altitude wind shear (Klingle et al. 1987). Sharp changes in both horizontal and vertical wind speed and direction across the front, in addition to turbulence created at the GF - outflow boundary, can cause tremendous catastrophes (Klingle et al. 1987). For example, they may negatively impact aircraft operations at terminals, vegetation and other structures such as homes and businesses.

Corresponding author address: Amber J. Liggett, National Weather Center Research Experiences for Undergraduates Program, Center for Analysis and Prediction of Storms, The University of Oklahoma, National Weather Center, 120 David L. Boren Blvd, Suite 2500, Norman, OK 73072 Email:amberliggett@yahoo.com

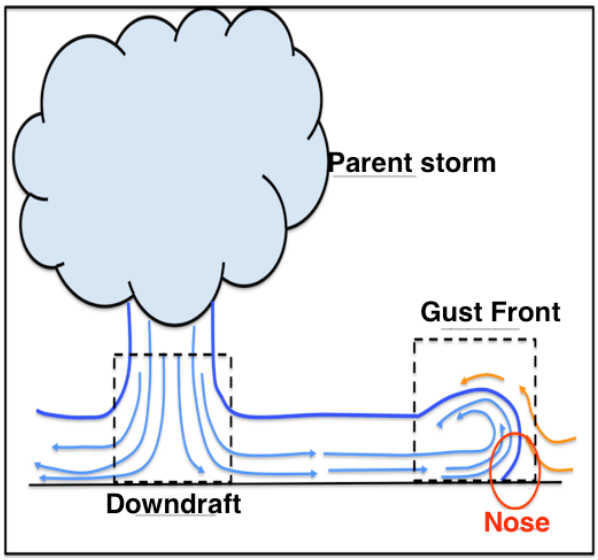

Figure 1. Schematic diagram of a GF, adapted from (Goff 1976). The parent storm is depicted by the cloud shape, and the blue arrows represent the flows from the parent storm. The orange arrows represent the flows of surrounding air, which are relatively warm and less dense. The regions of downdraft and GF are denoted as dotted boxes, respectively. The red circle shows the nose region of the GF and it is characterized by strong turbulence and wind convergence.

Already, Doppler radar, depicts the GF from enhanced spectrum width, a thin line feature in reflectivity, and convergence in velocity field (Uyeda and Zrnic 1985). The Machine Intelligence Gust-Front detection Algorithm (MIGFA), developed at the Massachusetts Institute of Technology (MIT) in 1993, is the current method of detecting GFs. Generally speaking, fuzzy sets are used to capture the signature of a thin line pattern in multiple radar fields (Delanoy and Troxel 1993).

The upgrade of the National Weather Surveillance Radar-1988 Doppler (WSR-88D) network to polarimetric capabilities was recently completed in 2013. Therefore this study of polarimetric GF signatures is timely. Having dual-polarization capability is essential for discriminating hydrometeor's types and between meteorological and non-meteorological scatters (Park et al. 2009). In general, WSR-88D scans at a range of 0–230 km, azimuth angles 0°–360°, and elevation scan angles of 0.5°–20° in approximately 4-5 minutes for storms (NOAA WDTB 2015).

Most recently, Hwang (2013) developed he Neuro-Fuzzy Gust-front Detection Algorithm (NFGDA) at the Advanced Radar Research Center (ARRC), University of Oklahoma and conducted a preliminary evaluation of the algorithm. Simply speaking, NFGDA is an artificial intelligence algorithm designed to emulate human decision-making for GF detection. NFGDA combines both Doppler and polarimetric signatures and their uncertainties using the Fuzzy Inference System (FIS). Moreover, the parameters in FIS are further optimized through a training process using the Neural Networks (NN).

Preliminary analysis with a limited number of cases has shown that NFGDA produced better performance than MIGFA. This study examined eight additional GF cases ranging in the mid-west and southeast during May and June in 2014 and 2015. There are two goals for this project. First, to verify polarimetric signatures of gust fronts. Then to conduct a performance analysis of the NFGDA, and to suggest refinements for the algorithm.

2. DATA and METHODOLOGY

2.1 *Procedure*

In this study, a compilation of severe weather events was obtained from NOAA Storm Prediction Center (SPC) Archives (http://www.spc.noaa.gov/exper/archive/events/index.html). This was used to identify gust front cases (time, date, and radar for each event) for this study. Subsequently, level-II base data from specific radar were downloaded from National Climate Data Center (http://www.ncdc.noaa.gov/nexradinv/map.jsp) (NCDC) NEXRAD inventory. Data from each of the eight cases was observed in NOAA Weather and Climate Toolkit 3.6.7. The radial properties used included the zeroth moment reflectivity (Z) at 0.51° scan angle in 24-hour format. In this study, eight cases of gust front, as listed in Table 1, with a total of 308 scans were analyzed.

2.2 *Method*

NFGDA was implemented in MATLAB_R2014a. The algorithm can be broken down to better understand the process in Figure 2.

Data Collection

Case	Radar ID	Location	Date	Volume Coverage Pattern (VCP)	# of Scans
I	KABR	Aberdeen, SD	Jun. 21, 2014	212	60
II	KDMX	Des Moise, IA	Jun. 30, 2014	12	22
III	KILX	Lincoln, IL	Jun. 21, 2014	212	29
IV	KJAX	Jacksonville, FL	Jun. 21, 2014	212	55
V	KLBB	Lubbock, TX	Jun. 13, 2015	12	31
VI	KLSX	St. Louis, MO	Jun. 21, 2014	12	21
VII	KSJT	San Angelo, TX	May 25, 2015	212	29
VIII	KVAX	Moody AFB, GA	Jun. 21, 2014	212	61

Table 1. A summary of the eight GF cases used in this work. Radar ID corresponds with the names of the WSR-88D sites, their locations are listed alongside the site names. These are all warm season events between May–June of 2014–2015. VCP range between 12 (severe convective events) and 212 (rapid evolving severe convective events). The total number of volume scans analyzed is 308.

In Figure 2, the input consists of crisp radar measurements Z, differential reflectivity (Z_{DR}), cross correlation coefficient (ρ_{HV}), radial velocity (V_r), and differential phase (ϕ_{DP}). Next, six variables including Z, line feature parameter (β), Z_{DR}, ρ_{HV}, SD(V_r), and SD(ϕ_{DP}) are computed in pre-processing. Note that β is a parameter, similar to one created at MIT for MIGFA, to characterize the line feature in Z and the motion of Z. Z_{DR} is defined from the ratio of power between horizontal and vertical channels, that can be used to identify a target's dominant shape. ρ_{HV} represents the similarity of signals from the two polarizations. SD(V_r) is the standard deviation of radial velocity, which was developed to characterize the convergence signature of the gust front. Moreover, SD(ϕ_{DP}) is standard deviation of differential phase, which can be thought of as the texture of differential phase. The NF system consists of a FIS and a NN training procedure. Subsequently, quality control and cleaning GF detections are performed in post-processing by examining the continuity of the preliminary detections from the NF system. Finally the output is a crisp value of 0 (non-GF) or 1 (GF) for each pixel.

A study by Hwang (2013) further explained how during pre-processing, each input field was converted to Cartesian coordinate system and both SD (V_r) and SD(ϕ_{DP}) were calculated. Additionally, the parameter β, that characterizes the line feature of reflectivity, was calculated using functional template correlation (FTC) (Hwang 2013). The line feature in Z, the motion of Z (defined by the difference of reflectivity fields from two consecutive scans) was obtained from the maximum value of the nine interest maps from nine rotational angles. Note that map rotation was done in the polar coordinate system, meaning that the map was rotated nine times and converted to the Cartesian coordinate system each time. After pre-processing, NF system decided whether or not there was a presence of GF based on the six variables at each pixel. The output of NF system was a binary detection result of either GF (1) or not (0). To suppress false detections caused by

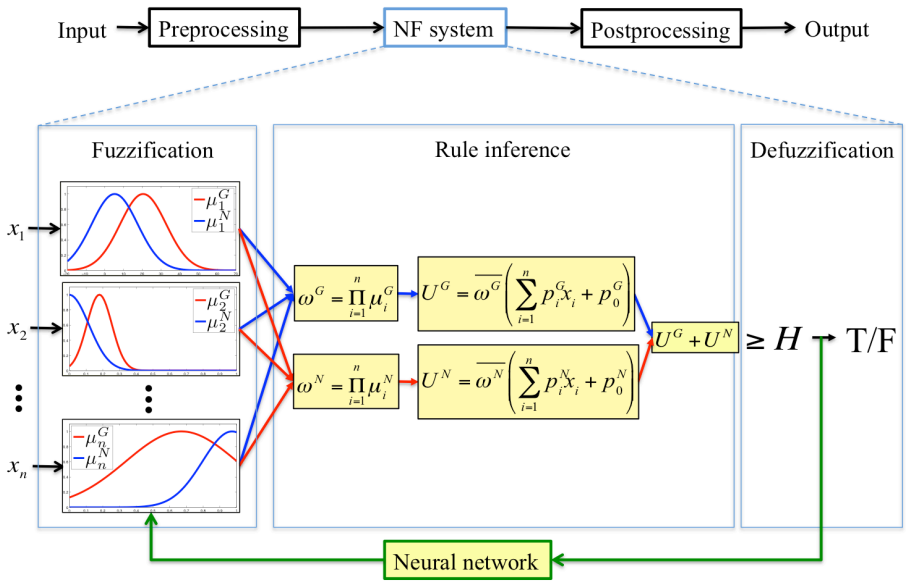

Figure 2. The NFGDA process with a detailed breakdown of the NF system.

noise or sometimes from the edge of the storm region, a quality control procedure was performed in post-processing. Consequently, a second-order polynomial fitting was applied to the location of detected pixels to obtain the GF location.

The term "fuzzy" refers to a non-threshold approach to classifying the condition as GF or non-GF based on multiple crisp inputs. Fuzzy logic was also used in the hydrometeor classification algorithm with polarimetric measurements (Park et al. 2009). Fuzzy logic can best be described as a variable term used in everyday language for human decision making. The familiarity of fuzzy logic, including terms such as high, medium, and low, is one more reason this feature is implemented in the algorithm.

The NF System consists of a FIS with three sub-sections, fuzzification, rule inference, and defuzzification as depicted in Figure 2. Under fuzzification, the six crisp inputs are converted to fuzzy sets for GF and non-GF. Then, fuzzy sets are combined in rule inference. In defuzzification, the rule inference fuzzy outputs are converted back to crisp outputs where the GF is represented by T for true and non-GF is represented by F for false.

Fuzzy logic is designed to detect GFs using membership functions (MFs). These MFs of the six input variables can be obtained initially from statistical analysis. Then, the NN makes fuzzy logic learn from training data, yielding a refined MF for a more accurate detection as demonstrated in Figure 3.1 and 3.2.

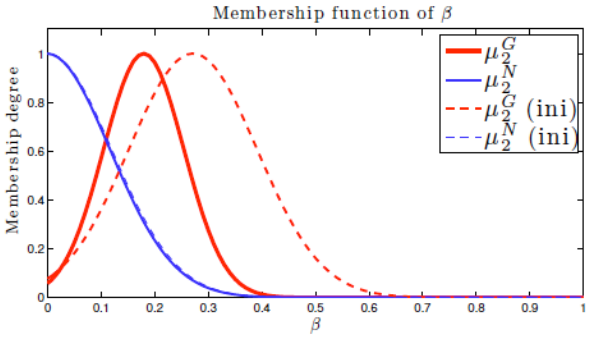

Figure 3.1. MF of *β*.

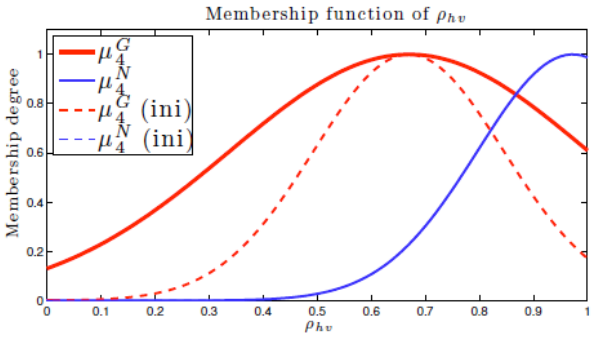

Figure 3.2. MF of ρ_{HV}.

In these figures, red lines represent the MFs for gust front (GF) and blue lines are for non-gust front (non-GF). The solid lines are MFs before undergoing NN while the dotted lines are MFs after being trained.

3. RESULTS AND DISCUSSIONS

Statistical results are represented in the normalized histograms in Figure 4.1–6, which highlight the GF signatures, red (GF) and blue (non-GF). Note that non-GF regions include those from clear air and storms.

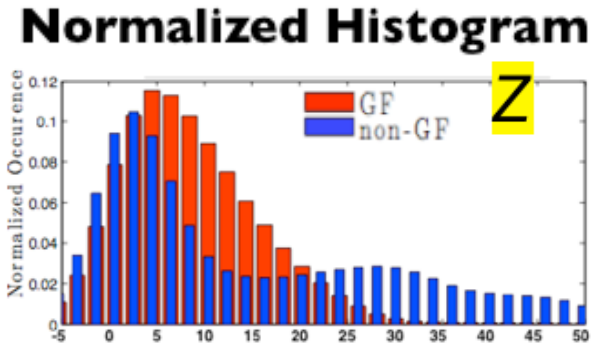

Figure 4.1. The normalized histogram for input variable Z.

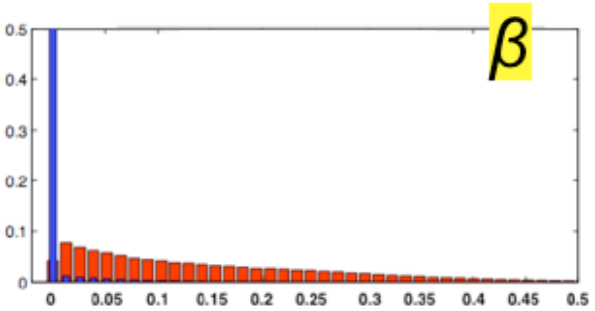

Figure 4.2. The normalized histogram for input variable *β*.

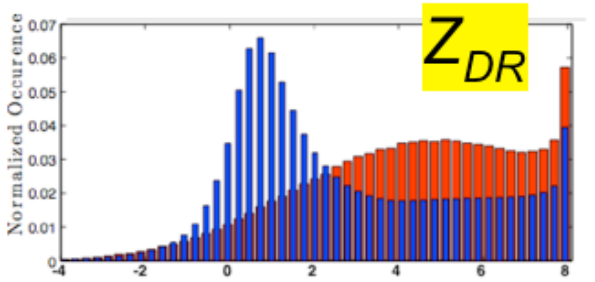

Figure 4.3. The normalized histogram for input variable Z_{DR}.

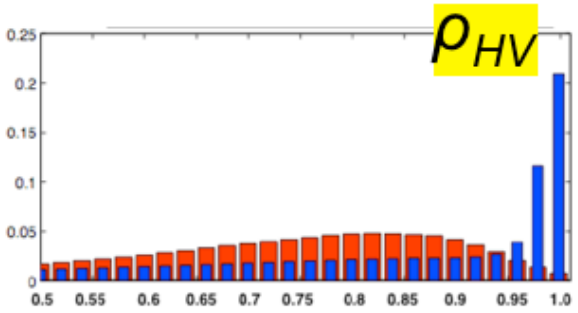

Figure 4.4. The normalized histogram for input variable ρ_{HV}.

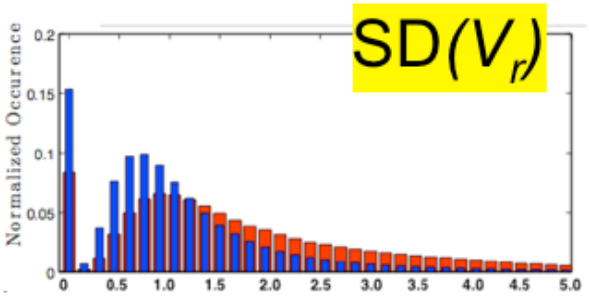

Figure 4.5. The normalized histogram for input variable SD(V_r).

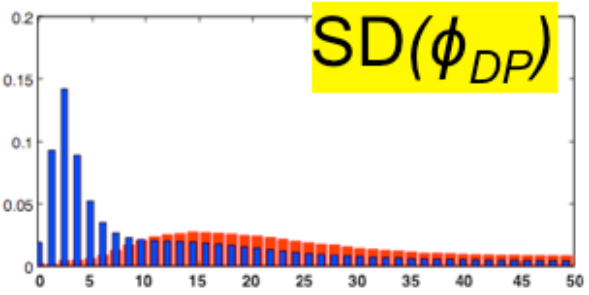

Figure 4.6. The normalized histogram for input variable SD (ϕ_{DP}).

The GF signatures are summarized as follows: low to medium Z, relatively high *β*, strong convergence SD(V_r), and polarimetric signatures include high Z_{DR}, low ρ_{HV}, and relatively large SD (ϕ_{DP}). The analysis results for these additional cases are similar to the preliminary results conducted by Hwang (2013).

In order to more thoroughly understand the cause of GF signatures, it is necessary to breakdown the structure of the GF in relation to the results from Figure 4.1–6.

The low to medium Z (5–15 dBz) in GFs as opposed to 40-50 dBZ in storms suggests a small

concentration of rain drops, and possibly non-meteorological scatterers such as insects, dust, etc. The relatively high β further confirms the thin line feature in reflectivity associated with GFs. In terms of Z_{DR}, a storm will yield a low 0–3 dB, while the GF generally produce high Z_{DR} of 4–8 dB. These results suggest that large rain drops and/or non-meteorological scatterers including insects with oblate shapes are present in GFs. The relatively low ρ_{HV} can be due to the mixture of different scatterers, for example, large raindrops or non-meteorological scatters. So generally ρ_{HV} is low, < 0.8 in GFs rather than high, 0.90–0.99 in a storm. A relatively high convergence, characterized by $SD(V_r)$, can be observed in GFs. Finally, the relatively high $SD(\phi_{DP})$ is attributed to the high ϕ_{DP} associated with insects frequently found in GFs as opposed to the low ϕ_{DP} of a storm (Zrnic and Ryzhkov 1998). It has been reported that frequently echoes from insects mark outflow regions of storms and transition zones between air masses with contrasting physical characteristics (Zrnic and Ryzhkov 1998). In other words, the polarimetric signatures of insects are beneficial for detecting GFs by NFGDA.

It is imperative to have the ground truth of GF location for the evaluation of NFGDA and the study of GF signatures. Ideally, the ground truth should be obtained from independent measurements. For the purpose of this study, a human expert first depicts a region of GF based on multiple radar data fields. As expressed by Hwang (2013), the location of all the pixels in the selected region was used to fit a curve using a second-order polynomial function. This curve is referred to as the true line. Subsequently, the true region is defined by the region centered at the true line with a width of 5 km. A true line is discussed in Figures 5.1-5.5. It is also denoted by the blue dashed lines shown in Figure 6, whereas the truth region is denoted by the yellow box of Figure 6.

Furthermore, the performance of NFGDA is evaluated quantitatively using the eight cases in Table 1, based on four detection scenarios of "hit", "miss", "false detection", and "correct rejection" as shown in Figure 5.

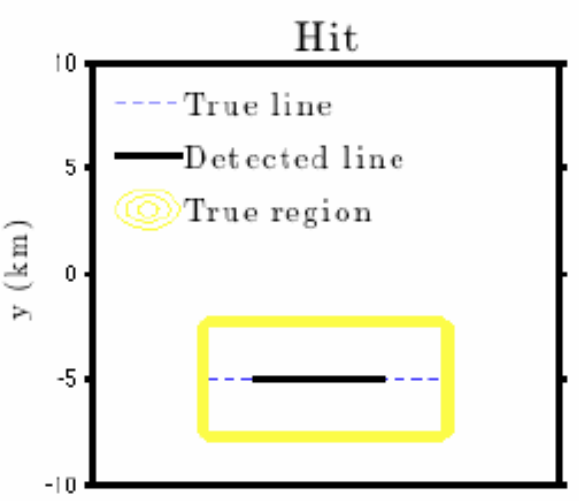

Figure 5.1. The ideal true line as defined by (Hwang 2013). This is the ideal scoring matrix used to evaluate the performance of both the NFGDA GF detection and human hand-picked GF region.

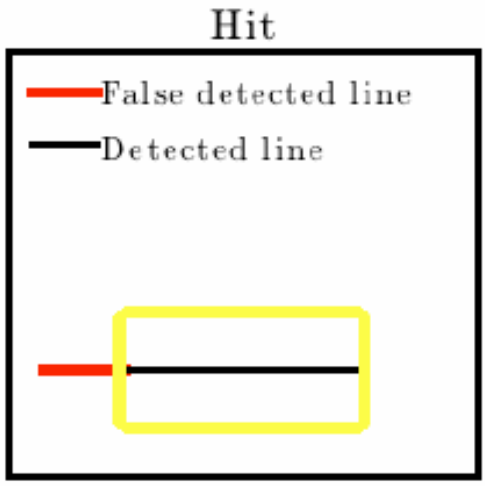

Figure 5.2. This is the "hit" component of the scoring matrix used to evaluate the performance of both the NFGDA GF detection and human hand-picked GF region.

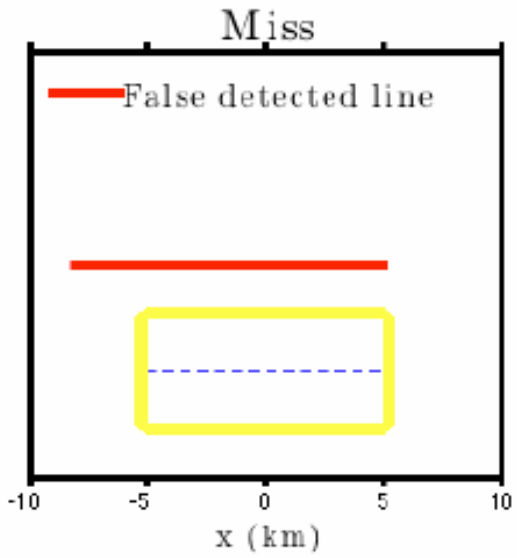

Figure 5.3. This is the “miss” component of the scoring matrix used to evaluate the performance of both the NFGDA GF detection and human hand-picked GF region.

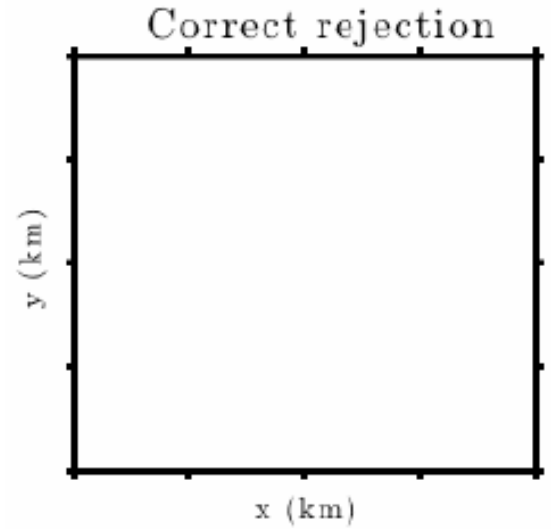

Figure 5.4. This is the “correct rejection” component of the scoring matrix used to evaluate the performance of both the NFGDA GF detection and human hand-picked GF region.

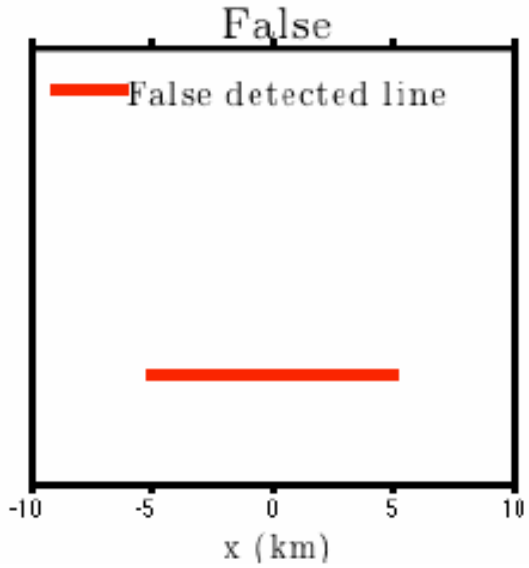

Figure 5.5.This is the “false” component of the scoring matrix used to evaluate the performance of both the NFGDA GF detection and human hand-picked GF region.

An ideal true line is denoted by the blue dashed lines shown in Figure 5.1, where the true region is denoted by the yellow boxes. A “hit” (Figure 5.2) is obtained when the dotted line from NFGDA lies fully or partially within the true region, as depicted by the solid lines in Figure 5.1 and 5.2. Note that the portion of the dotted line outside the true region is marked with red coloring. If the detected GF is completely outside of the true region then it is considered a “miss,” as shown in Figure 5.3. In addition to the GF cases, “correct rejection” (Figure 5.4) is defined when nothing is detected in null cases. However, if the line is detected without the true region, it is regarded as “false”, as shown in Figure 5.5 (Hwang 2013).

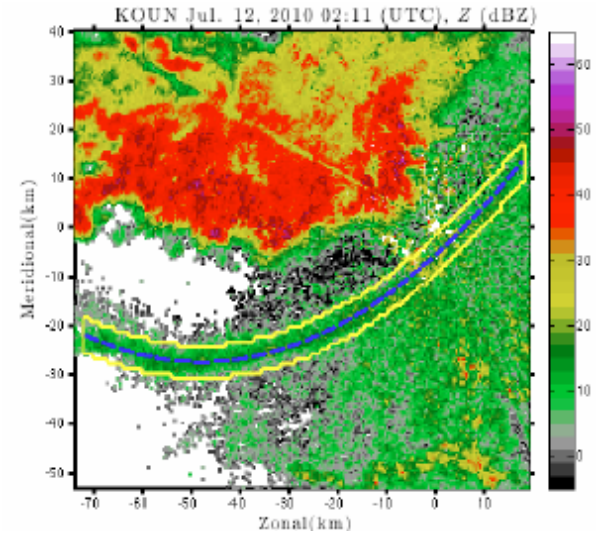

Figure 6.2. An example of ground truth from preliminary cases by Hwang (2013) for a GF is demonstrated. Locations selected by an expert are considered as truth and denoted by blue contours. A true region is depicted by the yellow box and is defined by extending the true line (blue dashed line) to 5 km. Within the hand-picked region is the thin line Z GF feature chosen by the human.

Then, as seen in Figure 7, there is a “hit” where the detected line lies in the truth region. Due to the low Z ~ 15–25 dBz, the remainder of the proposed GF region does not contain detected lines. Though not detected, the low Z falls under the GF signature for Z and should have been detected by the algorithm as a GF. This leaves room for future work in refining the algorithm and its sensitivity to low Z, and defining the GF region.

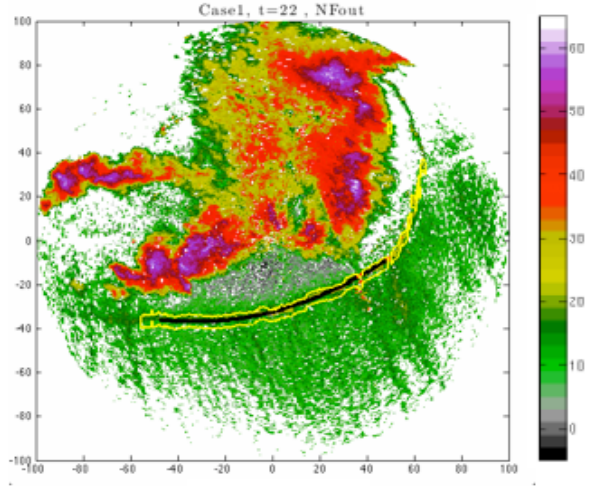

Figure 7. This image depicts the NFGDA detection from case I classified as a “hit”, because both the algorithm and human picked the region to have a GF. The hand-picked region is represented by the yellow lines.

Note, the earlier statement that the performance of NFGDA is evaluated quantitatively based on the four detection scenarios of “hit", “false", “miss", and “correct rejection". Consequently, the probability of detection (POD), the probability of false alarm (PFA), and the percent correct (PC) for the performance evaluation of NFGDA are provided in the following.

Probability of detections (POD) = $N_t / (N_t + N_m)$
Probability of false alarm (PFA) = $N_f / (N_t + N_f)$
Percent correct (PC) = $(N_t + N_r) / (N_t + N_m + N_r + N_f)$

where N_t, N_m, N_r, and N_f are the number of hit, false, miss and correct rejection for all the eight cases, respectively.

The final two measurements compare the length of correct detection and length of false detection, percent of length detection (PLD) and percent of false detection (PFD).

Percent of Length Detection (PLD) = L_t / L_{tot}
Percent of False Detection (PFD) = $L_f / (L_t + L_f)$

where L_{tot}, is the total length of the true line for all eight cases, L_t is the total length of detected line, and L_f is the total length of the portion of falsely detected line including over-detection, as shown in Figures 5.1–6.

The performance evaluation results are listed in Table 2.

Out of the total 308 volume scans analyzed, the algorithm and human expert detected the same truth region half of the time as the POD was 51.22% in Table 2. Limitations occurred as many of the GF cases had a propagation of a fairly weak Z ~ < 25 dBz. The algorithm did not detect the light thin line feature associated with the weak Z, primarily due to the algorithm’s sensitive nature and inability to detect the GF Z ~ < 25 dBz. For example, Figure 8 shows Case II which has a hand-picked region in a weak area of Z ~ 10–20 dBz that the algorithm failed to detect as a GF.

Method	POD(%)	PFA(%)	PC(%)	PLD(%)	PFD(%)
NFGDA	51.22	0	52.51	19.51	30.12

Table 2. The performance detection matrix results for the eight additional cases analyzed during this study. From left to right, probability of detection (POD), probability of false alarm (PFA) percent correct (PC), percent of length detection (PLD) and percent of false detection (PFD) are represented. The scores are in part due to the weak Z and the failure of the algorithm to detect that light Z feature.

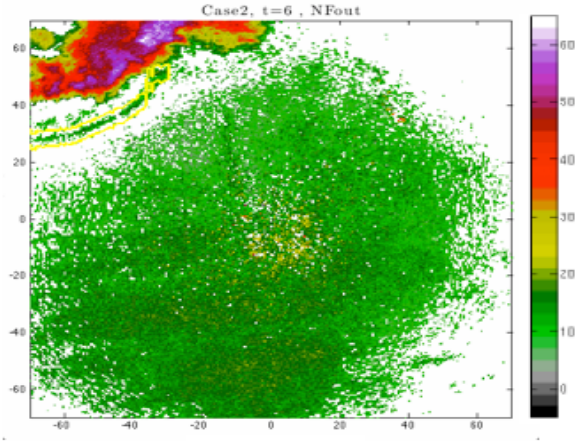

Figure 8. A "miss" hand-picked case due to weak Z.

4. CONCLUSIONS

Upon completion of implementing the NFGDA, results led to refinements in order to yield a more realistic performance evaluation.

There are challenges in defining the "true" GF/region. More specific guidelines can be placed in defining a GF, as it is not a well-defined storm feature. In order to alleviate this defect, the algorithm might need to be retrained.

Additionally, algorithm convergence signatures can be improved. For example, radial based convergence estimation can mitigate the smoothening of convergence as used in the standard deviation. NFGDA should be modified to handle cases of more than one gust fronts are present. For example, in Figure 9 there are two GFs propagating toward each other. If both GF regions could have been hand-picked, as opposed to only one, the NFGDA would potentially detect both leading edges as GFs. This could yield a higher performance evaluation detection.

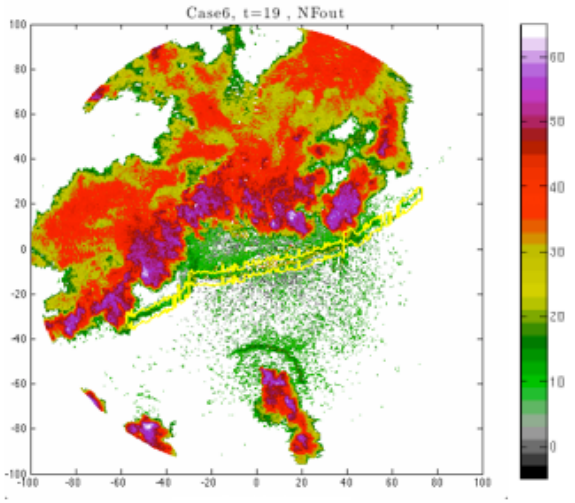

Figure 9. This image depicts the output of a time step from case VI where a GF region was hand-picked (within yellow true region), while another GF is propagating upward from a second parent storm (outside of true region).

The next step in analyzing the performance of NFGDA would be to conduct a performance evaluation in MIGFA to be compared with NFGDA results. Other future work may include highlighting polarimetric variables in NFGDA. One may even explore additional explanations for the weak Z feature, such as a lack of raindrops and insects.

Overall, the NFGDA is a promising algorithm in need of refinements to more accurately detect GF signatures.

5. ACKNOWLEDGEMENTS

I would like to acknowledge The Real World Research Experience for Undergraduates at The National Weather Center along with the Advanced Radar Research Center. Also, thanks to Dr. Daphne LaDue and Lori Wachowics for directing

the program, Yunsung Hwang, Ph.D. Candidate for the development and assistance with NFGDA. The National Science Foundation for funding the REU.

This material is based upon work supported by the National Science Foundation under Grant No. AGS-1062932.

6. REFERENCES

Achtemeier, G. L., 1991: The use of insects as tracers for “clear-air" boundary-layer studies by doppler radar. *J. Atmos. Oceanic Technol.*, **8**, 746-765.

Delanoy, R.L. and S.W. Troxel, 1993: Machine intelligent gust front detection. *The Lincoln Laboratory Journal*, **6**, 187-212.

Hwang, Y., 2013: Application of artificial intelligence to gust front detection with s-band polarimetric WSR-88D, M.S. thesis, The School of Meteorology, University of Oklahoma, 113 pp.

Klingle, D.L., 1985: A gust front case studies handbook, National Technical Information Service, 100 pp.

Klingle, D. L., D. R. Smith, and M. M. Wolfson, 1987: Gust front characteristics as detected by doppler radar. *Mon. Wea. Rev.*, **115**, 905-918.

Mueller, E. A. and R. P. Larkin, 1985: Insects observed using dual-polarization radar. *J. Atmos. Oceanic Technol.*, **2**, 49-54.

NOAA: Dual-polarization radar training for NWS partners. Accessed 25 June 2015. [Available online at http://www.wdtb.noaa.gov/courses/dualpol/Outreach/.]

NOAA: WSR-88D dual-polarization radar decision aid. Accessed 28 July 2015. [Available online at http://www.wdtb.noaa.gov/courses/dualpol/Outreach/DualPol-Flipchart.pdf.]

NOAA WDTB, 2015: Introduction to weather surveillance radar 1988 doppler (wsr-88d). Accessed 15 July 2015. [Available online at http://www.wdtb.noaa.gov/courses/dloc/topic2/rda/vcp.html.]

Park, H., A.V. Ryzhkov, D.S. Zrnic, and K. Kim, 2009: The hydrometeor classification algorithm for the polarimetric WSR-88D: description and application to an mcs. *Wea. Forecasting*, **24**, 730-748, doi: 10.1175/2008WAF2222205.1

Rinehart, R.E., 2004: RADAR For Meteorologists, Rinehart Publishing, 482 pp.

Skow, K., 2013: NWS wsr-88d radar fundamentals. Accessed 25 July 2015. [Available online at http://www.meteor.iastate.edu/classes/mt432/lectures/ISURadarTalk_NWS_2013.pdf]

Uyeda, H. and D.S. Zrnic, 1985: Automatic detection of gust fronts. *J. Atmos. Oceanic Technol.*, **3**, 36-50.

Zrnic, D. S. and A. V. Ryzhkov, 1998: Observations of insects and birds with a polarimetric radar. IEEE Trans. *Geosci. Remote Sens.*, **36** (2), 661-668.

Zrnic, S.D., V. M. Melnikov, and A. V. Ryzhkov, 2006: Correlation coefficients between horizontally and vertically polarized returns from ground clutter. *Bull. Amer. Meteor. Soc.*, **87**, 381-394.